An Amundsen Sea source of decadal temperature changes on the Antarctic continental shelf

Sybren S. Drijfhout[1,2,3] · Christopher Y. S. Bull[4] · Helene Hewitt[5] · Paul R. Holland[6] · Adrian Jenkins[4] · Pierre Mathiot[5,7] · Alberto Naveira Garabato[1]

Abstract

Mass loss from the Antarctic Ice Sheet is dominated by basal melting–induced warm ocean water. Ice-sheet mass loss and thinning of buttressing ice shelves occur primarily in the Amundsen and Bellingshausen Seas. Here, we show that in a global ocean simulation using the 0.25° Nucleus for European Modeling of Ocean (NEMO) model driven by the JRA55 reanalysis from 1982 to 2017, the Amundsen sector of the Antarctic continental shelf acts as a gateway, regulating the on-shelf access of warm Circumpolar Deep Water (CDW) from the deep ocean and its westward transfer to other sectors up to ca. 90° E, particularly the Ross Sea. As a result, anomalies in Antarctic-shelf-averaged temperature mainly originate in the Amundsen sector. These changes are primarily governed by shifts in the Amundsen Sea Low associated with tropical climate variability, modulating the on-shelf transport of CDW via wind-driven perturbations to ocean currents. The ensuing temperature anomalies progress westward from the Amundsen Sea via three distinct routes: a slow, convoluted westward pathway on the shelf via the Antarctic Coastal Current; a faster westward pathway along the shelf break via the Antarctic Slope Current and then onto the shelf along topographic troughs; and a third, eastward route toward the Bellingshausen sector, whereby temperature anomalies are transported into a region of local wind-generated changes farther north. These results emphasize the importance of the Amundsen sector for climate variability over the Antarctic shelves.

Keywords Amundsen Sea · Circumpolar Deep Water · Antarctic continental shelf · Subsurface warming · Global ocean model · Basal melt

✉ Sybren S. Drijfhout
s.s.drijfhout@soton.ac.uk

1 School of Ocean and Earth Science, University of Southampton, Southampton, UK

2 Royal Netherlands Meteorological Institute, De Bilt, The Netherlands

3 Institute for Marine and Atmospheric Research, Utrecht University, Utrecht, The Netherlands

4 Department of Geography and Environmental Sciences, Northumbria University, Newcastle upon Tyne, UK

5 Met Office, Exeter, UK

6 British Antarctic Survey, Cambridge, UK

7 University Grenoble Alpes, Grenoble, France

1 Introduction

Since the 1980s, the Southern Ocean has experienced subsurface warming extending to the Antarctic continental slope (Schmidtko et al. 2014; Meredith et al., 2019). This subsurface warming has likely been driven by increased upwelling of relatively warm Circumpolar Deep Water (CDW) leading to replacement of overlying fresher and colder waters (Schmidtko et al. 2014). In addition, the resulting stratification increase may have reduced mixing between CDW and near-surface waters, also causing CDW itself to warm (Bronselaer et al. 2020)—a mechanism consistent with model experiments (Jeong et al. 2020; Moorman et al. 2020). Closer to the Antarctic continent, Southern Ocean changes appear more complex. Especially in the Amundsen sector, water masses at depths of 400–1200m are 2–4 °C above local freezing temperatures (Dotto et al. 2019), inducing substantial basal melt of floating ice shelves, grounding line retreat (Rignot et al. 2013), and mass loss of the

glaciers connected to those ice shelves (Pritchard et al., 2012; Paolo et al. 2015). The warm water in the Amundsen Sea is sourced in upwelling CDW, but models and reconstructions of Amundsen Sea temperatures indicate that any weak warming signal is modulated by strong decadal variability (Jenkins et al. 2018; Naughten et al. 2022) driven by the tropical Pacific (Holland et al. 2019; Cai et al. 2023).

Farther north over and within the deep ocean, a long-term trend can be detected, both in the prevailing westerlies (Fogt and Marshall 2020) and in Southern Ocean temperatures, especially within CDW (Sallée 2018; Auger et al. 2021). The heterogeneous pattern of temperature change on the Antarctic continental shelf stands out from the stronger warming trend north of the continental slope. It has been argued that the presence or absence of the Antarctic Slope Front in any given sector plays a role in facilitating CDW access to ice-shelf cavities (Jenkins et al. 2016; Thompson et al. 2018), as does the occurrence of shelf-break undercurrents and deep canyon flows (Walker et al. 2013), overturning in coastal polynyas (St. Laurent et al., 2015; Webber et al. 2017), changes in sea-ice production (Timmermann and Hellmer 2013), and transient eddies (Thompson et al. 2018). Here, we use an eddy-permitting global ocean model including ice-shelf cavity flows and forced with an atmospheric reanalysis to examine how and where CDW enters the Antarctic continental shelf. Particular attention is given to what determines CDW delivery in this simulation: is it mediated by generalised upwelling around much of the Antarctic continent, or is along-shelf advection from other sectors particularly important?

2 Model and G07-JRA55 configuration

The spatial pattern of warming of the Antarctic shelves, its evolution over time, and the links with wind stress and ocean heat content (OHC) farther north are investigated by analysing a forced ocean-sea-ice run performed with an eddy-permitting global ocean model that allows for flow in sub-ice-shelf cavities (Mathiot et al. 2017). The ocean general circulation model used in this study is version v3.6 of the Nucleus for European Modeling of Ocean (NEMO) model (Madec 2016), with sea-ice model LIM-3.6 (Rousset et al., 2015). The model used here is the global, 1/4° (horizontal resolution) NEMO 'G07' configuration (Storkey et al. 2018) developed by the Met Office Hadley Centre. New in the G07 model is the utilization of an ice-shelf module. In the present set-up, the ice shelf is assumed to be in equilibrium, with the mass removed by melting being replenished by flowing land-ice, keeping the shape of the sub-ice-shelf cavity constant over time. The impact of including the ice-shelf cavities has been evaluated in a circum-Antarctic version of the eNEMO model (Mathiot et al. 2017). The fresh water and heat fluxes

resulting from ice-shelf melting are specified at the ice shelf/ocean interface; that is, they are prescribed and not interactively calculated. The specification of ice-shelf melting over the area of the ice-shelf base follows Rignot et al. (2013). Prescribing ice-shelf melting instead of calculating it from simulated ocean temperatures leads to major improvements in the water mass properties, ocean circulation, and sea-ice state on the Antarctic continental shelf (Mathiot et al. 2017). Meltwater is treated as a volume flux; that is, it affects the ocean flow divergence near the ice draft. To reduce model drift, our model, G07-JRA, applies sea surface salinity restoring north of 55° S at the same time minimizing the effect of salinity restoring on the Southern Ocean (Mathiot et al. 2017). The model used here is the same as described in Storkey et al. (2018), to which we refer for more details on the model. The forcing data used here, however, is different, namely the 55-year Japanese Reanalysis for driving oceans 'JRA55-do' (Tsujino et al. 2018). Like in Storkey et al. (2018), the forced ocean-sea-ice model is initialized on January 1, 1976, from version 4 of the Met Office Hadley Center objective analysis dataset 'EN4' (Good et al. 2013), and run with JRA55 forcing without a preceding spin-up. Although the JRA55 reanalysis starts in 1958, data prior to 1976 over the Southern Ocean are estimated as too sparse for a reliable reanalysis over that area. Output of the G07-JRA has also been used to study the impact of ocean dynamics on the Filchner-Ronne (Bull et al. 2021).

3 Model evaluation

In our analysis, we define the boundaries of the continental shelf to be the limit of the grounded ice in the south and the 1000-m isobath in the north. The continental slope is taken as a band of 2° in latitude north of the shelf edge. In the first 6 years (1976–1981), the shelves generally become colder and fresher, while the upper ocean just north of the shelves becomes warmer and more saline (Fig. 1). It could be that either missing ocean processes or the atmospheric forcing does not support the amount of CDW on the shelves contained in the initial conditions and or that the initial conditions are somewhat biased to summer values and (warmer) later years. In the remainder of our analyses, the first 6 years of the run have been disregarded, thereby reducing the impact of model drift. Fig. 2 shows time series from 1982 onwards of the horizontally and vertically averaged temperature anomaly for the Antarctic shelf and for the Bellingshausen, Amundsen, and Ross sectors separately, relative to their 1982–2017 mean. Decadal temperature variations are much more prominent than any trend over this 35-year period. Because trends between 1982 and 2017 are larger over the continental slope and farther north, all data hereafter is linearly detrended to allow a better view
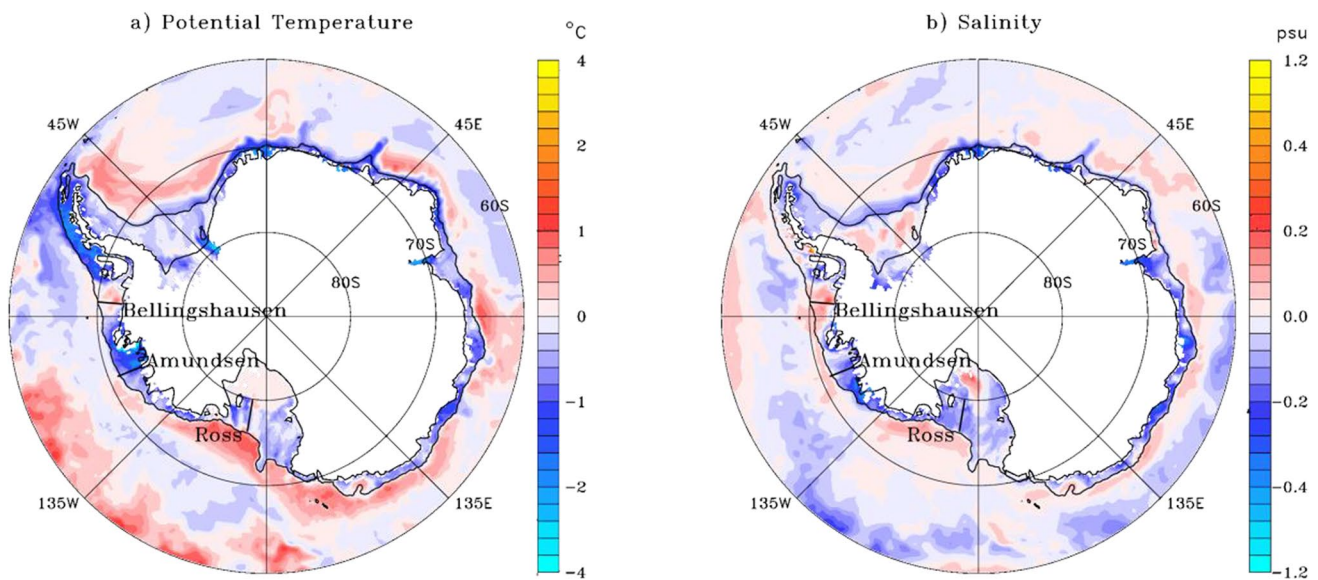
a) Potential Temperature

b) Salinity

Fig. 1 Difference between simulated **a** potential temperature and **b** salinity between year 1981 and the initial model state in 1976 (EN4). Fields are averaged over 0–800 m depth or bottom level when depth is less than 800 m. We acknowledge that the land/sea mask in the plotting software does not contain the latest information on ground-

ing lines showing for instance ocean temperature and salinity in the Weddell Sea beyond the land boundary which reflects the ice front, missing the ice cavity. We assume that this is not hampering the interpretation of this and following figures in the manuscript
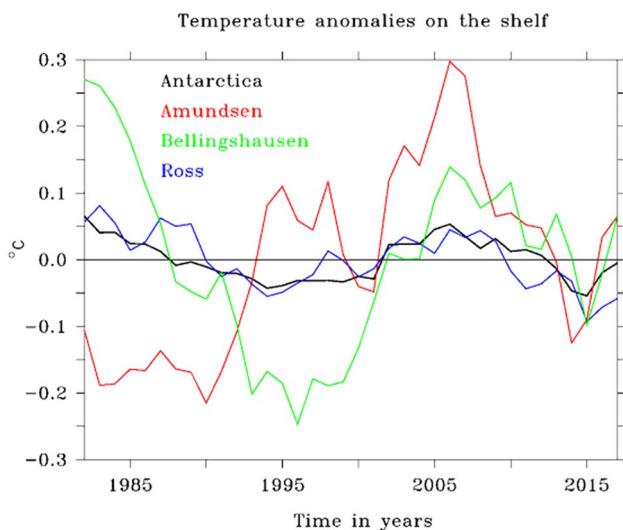

Fig. 2 Time series of basin-averaged temperature anomaly, with respect to its 1982–2017 average, of the circum-Antarctic shelf and three indicated subbasins including ice cavities

of how anomalies in the Southern Ocean may upwell over the continental slope and flood the continental shelf. Further analysis in this paper is thus performed on the period 1982–2017 in which also the non-detrended data show no detectable drift on the Antarctic shelves. When focusing on the subsurface, the comparison with observations improves (compare Fig. 3 with Fig. 2 from Jenkins et al. 2016). Here, we have chosen to use a similar colour scheme as used in

Fig. 2 of Jenkins et al. (2016), although it should be noted that these authors use a slightly different observational dataset to compare with (Orsi and Whitworth 2005). There is a temperature and salinity bias on the Antarctic shelf (Fig. 1), but the bias is mainly in the upper 400 m. In the 400–1200-m layer, the overall water mass structure on and north of the shelves in the Southern Ocean compares well with observations (Fig. 3). Further information on model performance is given in Supplementary Fig. 1 showing the barotropic streamfunction and annual-mean sea-ice cover maps averaged over years 1982–2017.

In Fig. 4, we zoom in on cross sections in the Ross, Amundsen, and Bellingshausen Seas (see Fig. 3 for the location of these sections). Shown are the varying meridional structure of the westward-flowing Slope Current and/or Antarctic Coastal Current flowing on the shelf, on three areas of the Antarctic shelf, and the eastward undercurrent that develops in the Amundsen Sea. The simulated Slope Current and undercurrent are in qualitative agreement with observations (Walker et al. 2013; Jenkins et al. 2016; 2018) including the undercurrent's turning southward on the Amundsen sector of the shelf (Assmann et al. 2013). The left panels in Fig. 4 compare well with the temperature and salinity structure displayed in Fig. 6 from Walker et al. (2013), section A, but the simulated undercurrent is about a factor of 2 too weak. High-resolution meridional sections in the central and eastern Ross Sea are much scarcer in the literature, but the temperature section of Fig. 4 can be compared to the Drygalski section (Fig. 1)
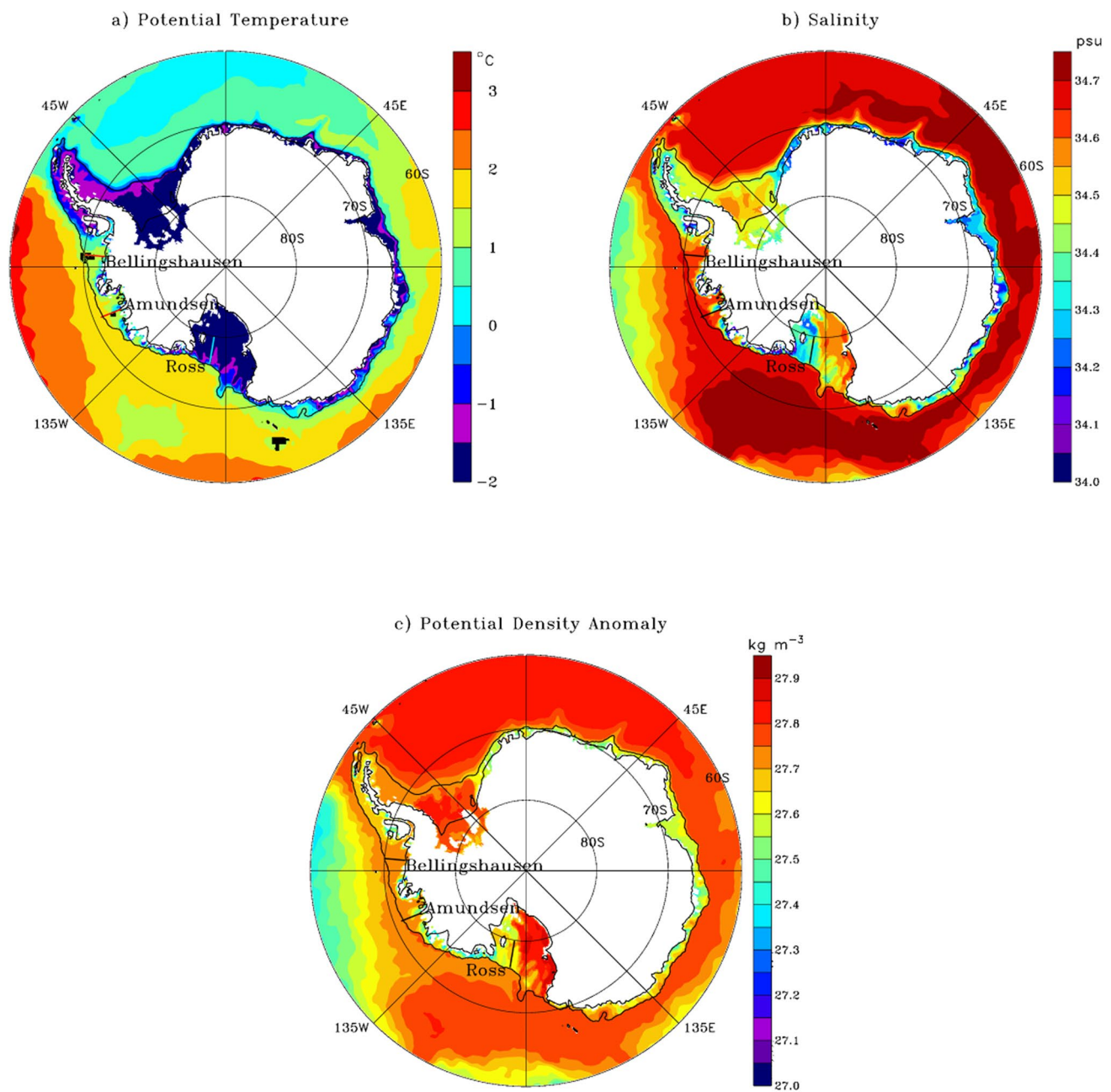
a) Potential Temperature

b) Salinity

c) Potential Density Anomaly

Fig. 3 Model simulated **a** potential temperature, **b** salinity, and **c** potential density anomaly (− 1000) averaged over 400–1200 m depth or 400 bottom level when depth is less than 1200 m or bottom level value when depth is less than 400 m. Location of meridional sections displayed in Fig. 4 for the Bellingshausen, Amundsen, and Ross continental shelves is indicated, as well as the 1000-m isobath that coincides with the shelf edge

in Bowen et al. (2021), showing good agreement. For the Bellingshausen sector of the shelf, more sections are available, although not as much data as for the Amundsen sector. Fig. 5 can be compared to Jenkins and Jacobs (2008), their Fig. 2, and shows good agreement. We conclude that the main water mass structure in the Southern Ocean just off and on the shelf are well represented in the model, and the main currents on the slope and shelf are present if possibly too weak, but this should not affect the qualitative picture sketched here.

Time series of basin-averaged temperature anomaly for the Antarctic shelf and various separate sectors show largest-amplitude variations in the Amundsen sector. These consist of a cool period till 1990, followed by warming till the mid-1990s, cooling till ca. 2000, further warming till ca. 2007, cooling till 2014, and warming resuming till 2017 (Fig. 1).
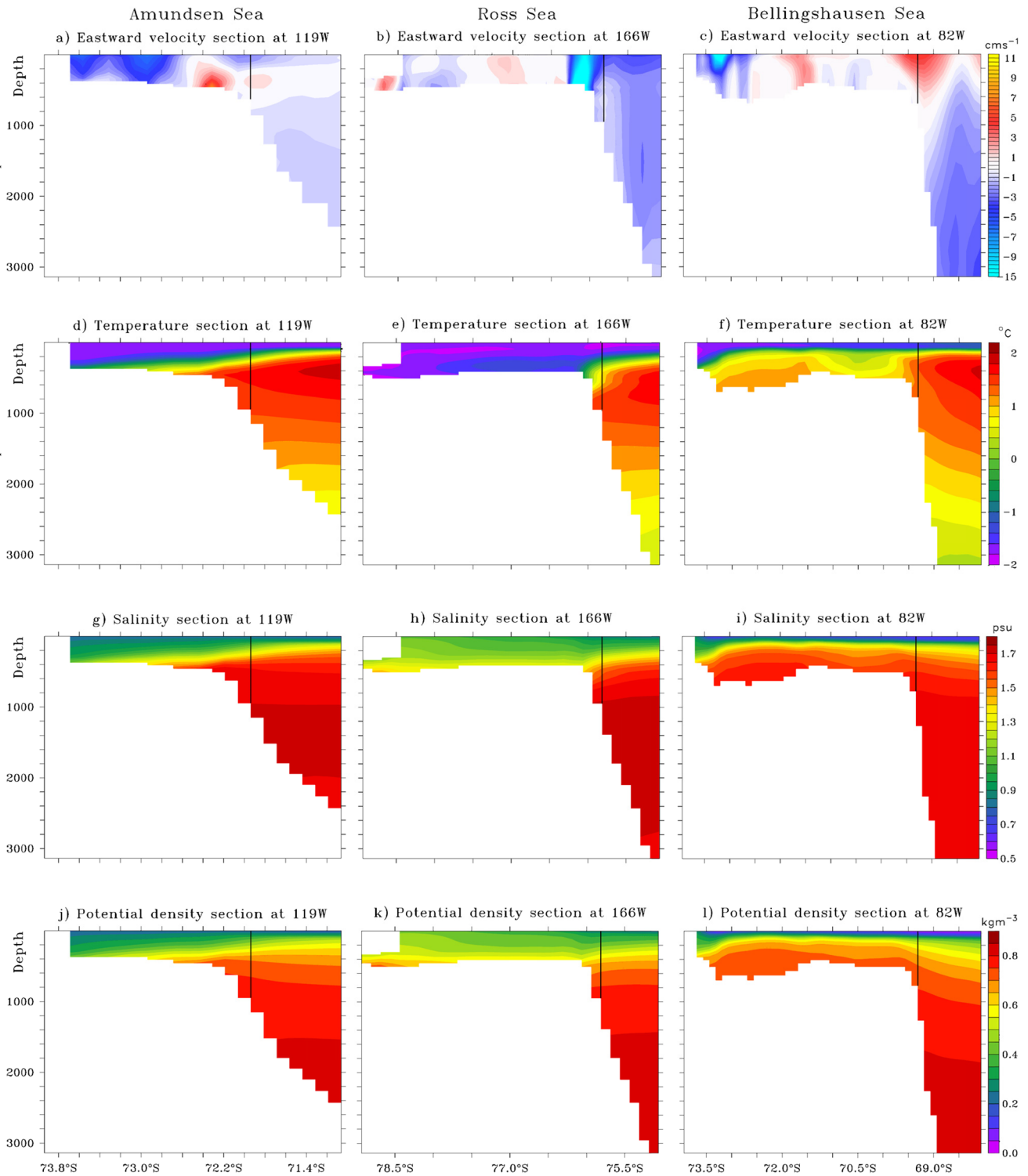
Fig. 4 Meridional sections across the continental shelf and slope of **a–c** eastward velocity, **d–f** potential temperature, **g–i** salinity 33 psu, and **j–l** potential density minus 1027 kg m^{-3} s^{-1} at 119.1° W (left panels), 166.1° W (middle panels), and at 82.6° W (right panels)

This signal is in rough agreement with a previous assessment that ocean forcing from the tropical Pacific drives changes in upwelling (Jenkins et al. 2016; 2018; Jeong et al. 2020)

and wind variations in the eastern Amundsen Sea (Holland et al. 2019) (compare, e.g. their Fig. 5 with Fig. 1). The modelled Antarctic Circumpolar Current is somewhat weaker

Fig. 5 Time series of **a** Antarctic Circumpolar Current in Sverdrup ▶ defined as eastward volume transport at 66° W; **b** Antarctic Bottom Water Cell defined as overturning streamfunction defined at 30° S; **c** Ross gyre defined as barotropic streamfunction minimum between 155° W and 140° W minus westward transport at 160° W; **d** Weddell gyre as barotropic streamfunction minimum between 12.5° W and 5° E minus westward transport at 55° W; and **e** yearly average Southern Hemisphere sea-ice area

than recent estimates based on observations (Fig. 5a), but well within the range of present-day models. The simulated deep overturning (Antarctic Bottom Water) cell (Fig. 5a, b) shows mean values well within observational uncertainty limits. Both time series show a clear downward trend, probably associated with the model's inability to form realistic amounts of Antarctic Bottom Water, a common problem in climate and ocean models (Heuzé, 2021).

The modelled Ross and Weddell gyres (Fig. 5c, d) have realistic strength and interannual variability, as far as can be assessed from observations, and no clear trends (Dotto et al., 2019; Neme et al. 2021). The time series of sea-ice extent (the integral sum of the areas of all grid cells with at least 15% ice concentration (Fig. 5e)) compares well with observations, although sea-ice area is too weak in the model, due to too less sea ice in summer (not shown).

4 Results

4.1 On-shelf temperature anomalies start in the Amundsen sector

Visual inspection of Fig. 2 suggests that shelf-averaged variations (black curve) in the Ross sector (blue) and Bellingshausen sector (green) are correlated. Variations in the Amundsen sector (red curve) start with a cool period, followed by a warm period before this sequence is seen elsewhere, but after year 2000, the variations in the Amundsen sector appear to join those in other sectors. The cycle of variability in this period has a time scale of about 25 years, implying that the model resolves only one cycle. In the remainder, we examine the sequence of events during 1982–2017 without claiming that the phasing during 1981–2017 also holds for other periods.

Here, we use a lagged-regression analysis (Supplementary Table 1) to explain the different timing of warm and cold anomalies in different basins as shown in Fig. 2. To this end, we analyse whether this is due to a different timing of CDW delivery to different sectors by lags in upwelling to these sectors from the deep ocean or by redistribution of CDW on the shelf after upwelling at preferred sites. This would help us answer how and where CDW enters the Antarctic continental shelf. Fig. 6 shows the lagged regression of vertically averaged temperature on the Antarctic continental
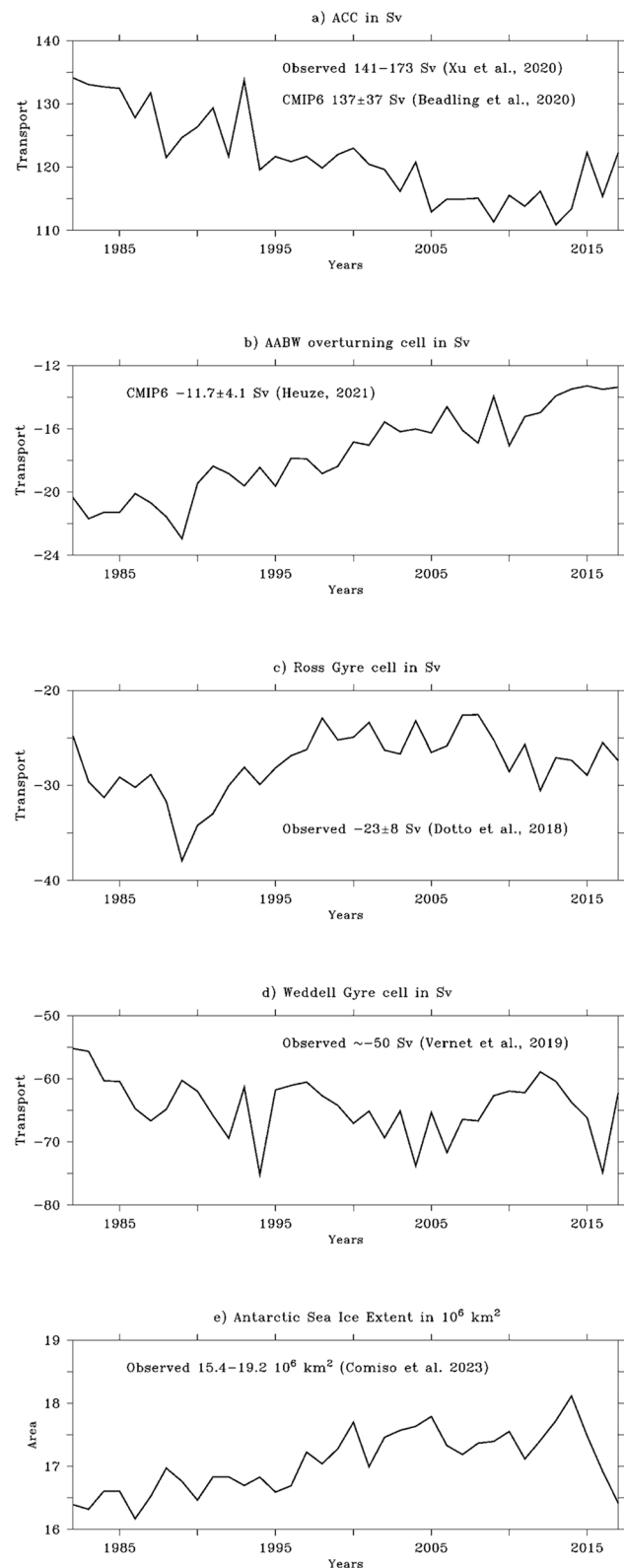
shelf to the shelf-averaged temperature. The regression indicates that decadal temperature variations are initiated in the Amundsen sector. Nine years before temperature anomalies
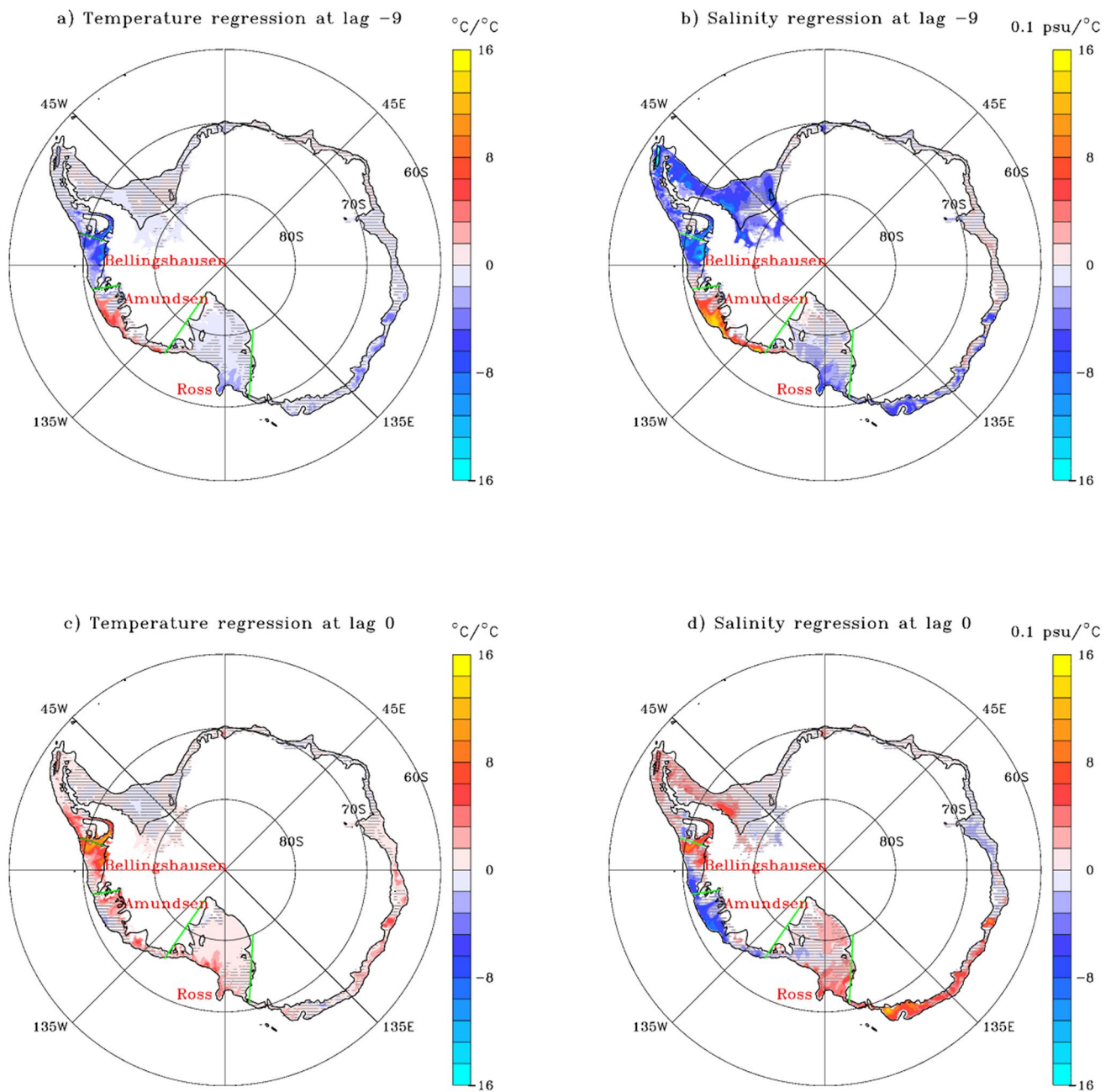
Fig. 6 Regression of **a**, **c** vertically averaged temperature on the shelf and **b**, **d** vertically averaged salinity anomaly on the shelf, on circumpolar and vertically averaged temperature anomaly on the shelf. **a**, **b** At lag − 9 years (units °C °C^{-1} and 0.1 psu °C^{-1}). **c**, **d** At lag 0. Non-significant values according to a two-sided Student T-test are overlaid by grey horizontal lines

on the whole shelf peak, a temperature anomaly of the same sign is visible in the Amundsen sector (Fig. 6a), with anomalies of opposite sign elsewhere. In the following 9 years, this anomaly progresses westward to the Ross Sea and farther west up to 90° E and then also appears east of the Amundsen sector in the Bellingshausen sector (Fig. 6c). When the Antarctic shelf-averaged temperature anomaly peaks, almost all sectors west of the Peninsula till 90° E exhibit a temperature anomaly of similar sign (Fig. 6c). The anomaly's

amplitude is largest in the Bellingshausen sector and clearly visible west of the Bellingshausen sector as far as 90° E (the anomaly is weak or non-existent between 90° E and the Antarctic Peninsula). Considering a warming phase, the initial anomaly in the Amundsen sector can be associated with a larger intrusion of warm and salty CDW, while the rest of the shelf is still cold and fresh (Fig. 6a, b). When the shelf-averaged temperature peaks, positive salinity anomalies are found eastward of the Amundsen sector up to 90° E and

westward of the Amundsen sector (Fig. 6d). The Amundsen sector itself is then characterised by negative salinity anomalies, while the temperature anomalies are still positive. An overview of the regressions performed is presented in Supplementary Table 1.

Because the regression is linear, the storyline reverses for a cooling phase on the Antarctic shelf. The suite of regressions gives additional context to Fig. 2. The shelf-averaged temperature (black line in Fig. 2) is indeed dominated by temperature changes in the Bellingshausen and Ross sectors (green and blue lines). Before year 2000, temperature change in the Amundsen sector (red line) appears to lead temperature change in other sectors, and this lead is confirmed by the regression maps. Anomalies in the Amundsen sector occur ca. 9 years before they peak in other sectors, and in Fig. 2, we see indeed the negative temperature anomaly in the Amundsen Sea from the late 1980s appearing ca. 9 years later in other sectors. The same appears to hold for the positive anomaly in the late 1990s, appearing ca. 9 years later in other sectors. However, because the negative anomaly around year 2000 only lasts for 2–3 years in the Amundsen Sea, the positive anomaly between 2002 and 2012 also coincides with (and possibly precedes by a few years) the positive anomaly in other sectors, which still is the 9-year lagged response to the positive anomaly of the late 1990s in the Amundsen Sea (assuming a fixed travel time of the anomaly of ca. 9 years to both Bellingshausen and Ross sectors). Of course, we cannot prove that this 9-year lag between the Amundsen and other sectors is a robust and constant feature from the short time series shown in Fig. 2. It is obvious that when the forcing of the Amundsen Sea has a time scale equal to, or shorter than, the travel time of anomalies from the Amundsen Sea to other sectors, the lag is no longer discernible from time series alone. We stress that we do not claim that the phasing we deduce from this time series always applies; it merely describes the sequence of events in the period 1982–2017.

4.2 Temperature anomaly propagation on the shelf and slope

To further substantiate the westward propagation of temperature and salinity anomalies inferred from Fig. 6, we present Hovmöller diagrams for three different depth ranges: 200–400 m, 400–600 m, and 600–800 m (Fig. 7). The 600–800-m layer intersects with the bottom topography. The 0–200-m layer is affected by air/sea interaction and surface forcing of the anomalies and is not considered. We analyse three layers anticipating that propagation pathways and speed vary in the vertical, considering even more layers would complicate presentation and interpretation of the results. Supplementary Fig. 2 shows the vertical distribution of temperature anomalies when averaged temperature peaks.

Westward propagation of temperature anomalies on the shelf and slope is visible in the Amundsen and Ross sectors between 120° W and 170° E (Fig. 7). In the 200–400-m layer (Fig. 7a, b), where anomalies peak, and in the 400–600-m layer, there is evidence for slower propagation between 100° W and 170° E of ~ 90° in 7 years (~ 1.5 cm s^{-1}) and faster propagation between 170° E and 40° E of ~ 130° in 3 years (~ 5 cm s^{-1}). Oblique, straight black lines, matched by the eye in these panels, connect anomalies that are consistent with above-mentioned propagation speeds.

The Rossby wave speed on the shelf is very small O (1 mm/s), because beta decreases with increasing latitude and the Rossby radius on the shelf is only a few kilometers, more than 10 times smaller than in the midlatitude ocean. Thus, we infer that westward propagation speeds of temperature anomalies of ~ 1.5 and ~ 5 cm/s must be due to mean flow advection. Inspection of the velocity map in the 200–400-m layer (Fig. 8a) reveals that a highly convoluted pathway on the shelf exists for anomalies to reach the Ross sector, but this pathway includes substantial meridional steering by complex shelf topography. Zonal flow on the shelf is westward in the Amundsen and Bellingshausen sectors (Figs. 4a, c and 8a, b). In the 200–400-m layer, this flow is associated with the Antarctic Coastal Current that strongly meanders, steered by meridional flows in deeper troughs (Fig. 8a). This flow becomes weaker in the 400–600-m layer (Fig. 8b) and a direct pathway to the Ross sector no longer exists as below 400 m, the layers start to intersect with the bottom. Anomalies advected via the direct pathway in the 200–400-m layer must therefore also feed the 400–600-m layer possibly via downward advection and mixing, as the slower propagation mode is visible in this layer as well (Fig. 7c, d). In the Ross sector, westward flow is weaker and northward and southward currents dominate (Figs. 4b and 8a, b). However, along the slope on the eastern side of the Amundsen sector and in the Ross sector, the faster Antarctic Slope Current develops (Figs. 4b and 8a). The slow and fast modes of propagation are roughly in agreement with the mean westward velocities on the shelf and slope (Figs. 4a–c and 8a, b).

The 600–800-m layer starts to intersect with the bottom on the shelf. Here, westward propagation on the shelf is inhibited by topography (Figs. 7e, f and 8c) and anomalies are confined to isolated troughs, leading to a Hovmöller diagram with white longitudinal bands where the bottom is shallower than 600 m. Westward propagation can still be detected, associated with the more continuous signal on the slope, where the bottom is below 800 m (Fig. 7e, f). There, anomalies propagate almost exclusively with the fast advection speed of ~ 5 cm s^{-1}, and the propagation signal is less ambiguous than in the 200–400-m and 400–600-m layers. In the 600–800-m depth range, anomalies primarily propagate via the Antarctic Slope Current and are intermittently transferred onto the shelf via deep canyons (Fig. 8c).
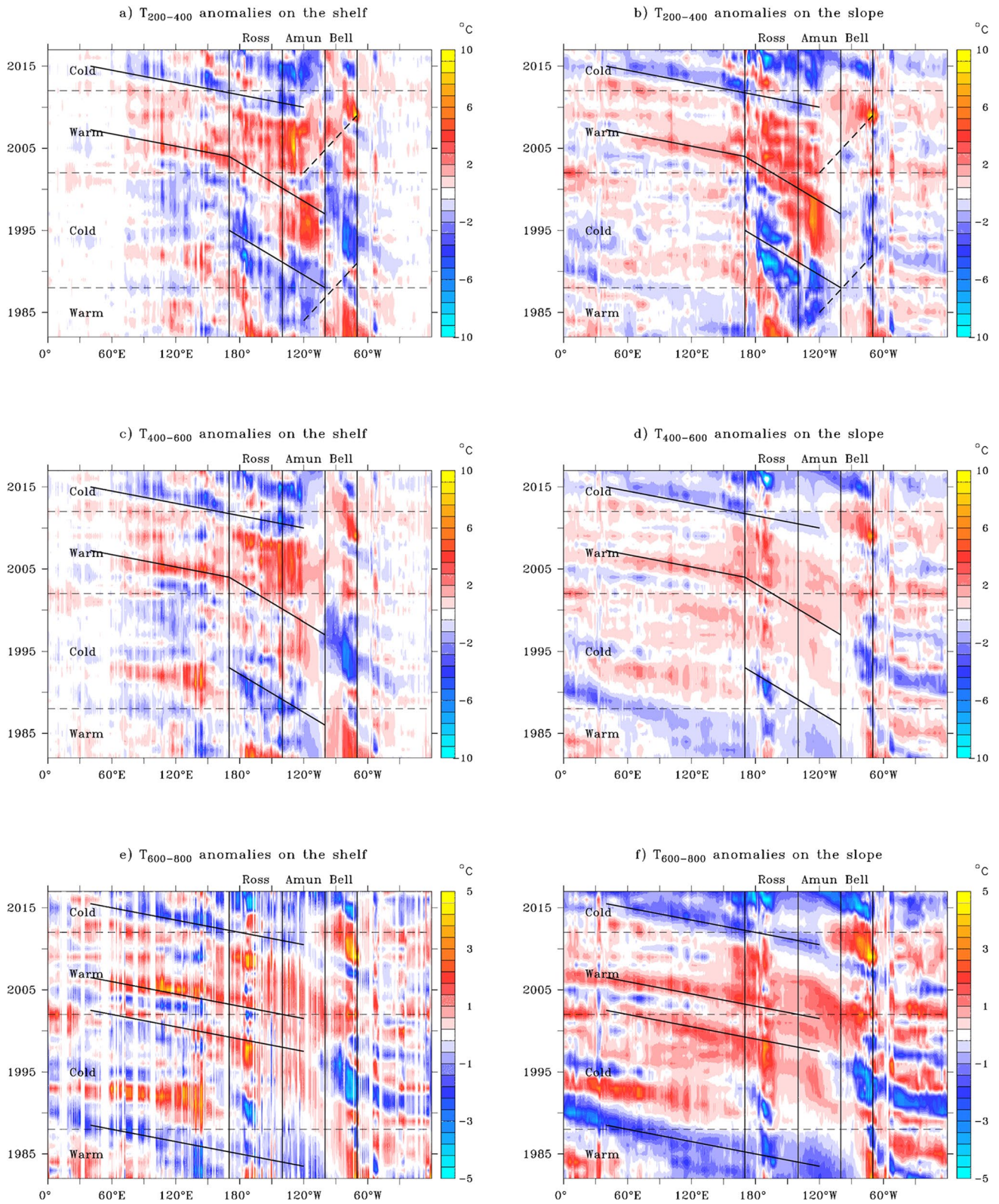
Fig. 7 Hovmöller diagrams for **a**, **c**, **e** temperature anomalies on the shelf averaged over a 1° latitude width, just south of the shelf edge and **b**, **d**, **f** for temperature anomalies at the continental slope averaged over a 1° latitude width, just north of the shelf edge (units 0.1 °C). **a**, **b** Two hundred to 400-m depth average; **c**, **d** 400–600-m depth average; **e**, **f** 400–600-m depth average. Black vertical lines indicate the boundaries of the Ross, Amundsen, and Bellingshausen sectors. Oblique lines indicate propagation, with steeper slopes showing slower propagation. Solid oblique lines indicate westward propagation and dashed oblique lines eastward propagation. Horizontal dashed lines divide time in periods of anomalous warm and cold episodes on the Antarctic shelf based on Fig. 2
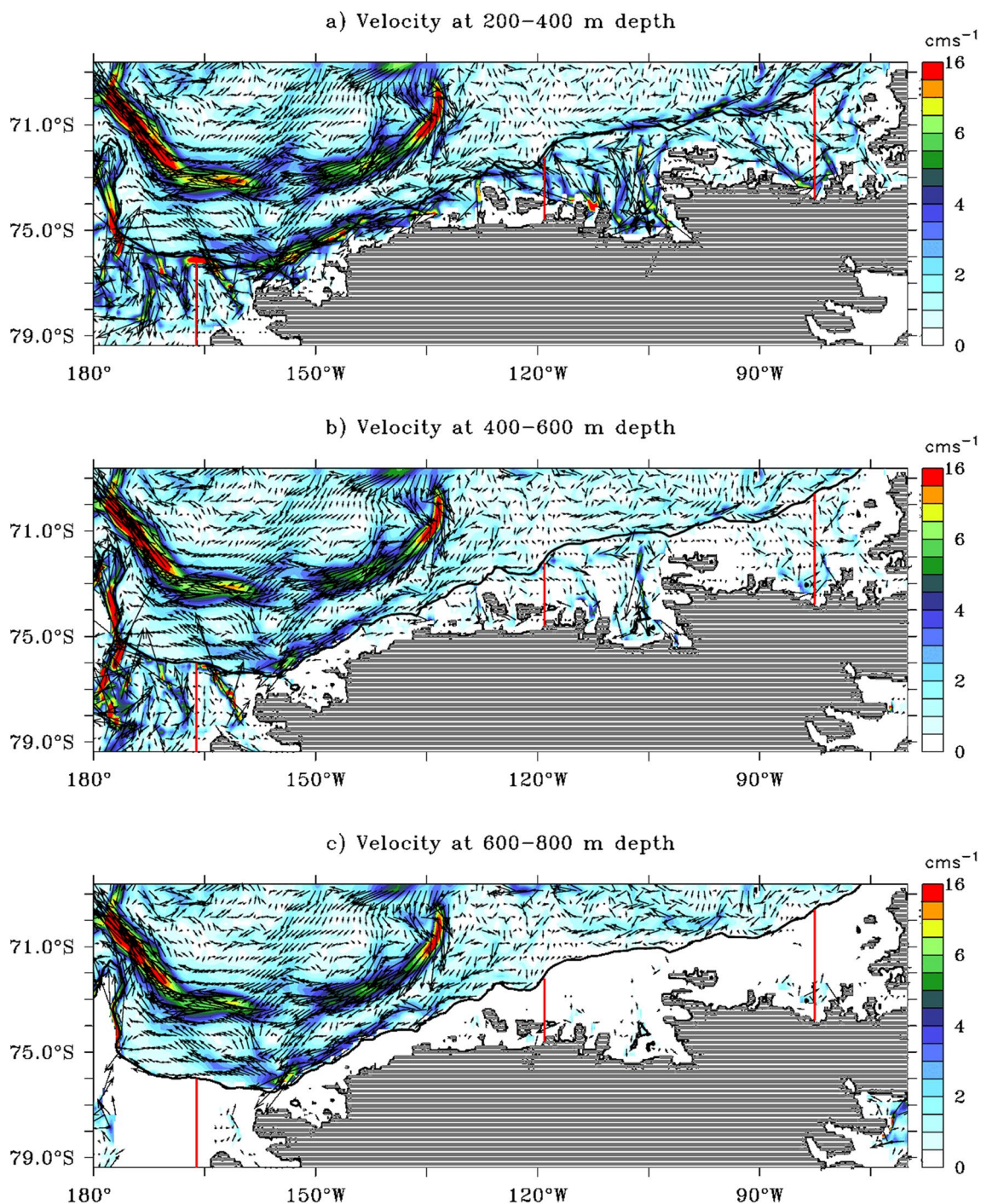
a) Velocity at 200−400 m depth

b) Velocity at 400−600 m depth

c) Velocity at 600−800 m depth

Fig. 8 Time-average velocity field **a** averaged over 200–400 m depth, **b** averaged over 400–600 m depth, and **c** averaged over 400–600 m depth. The continent is indicated by grey horizontal lines. Location of meridional sections displayed in Fig. 4 are indicated by red lines

Propagation via the Antarctic Slope Current in this layer is supported by maps of time-mean velocity vectors, which indicate that there is no continuous zonal flow on the shelf at depths of 600–800 m, such that westward propagation must occur via the flow along the slope which indeed is ca. 5 cm s^{-1} (Figs. 4b and 8c).

There are also subtle indications of eastward propagation of temperature anomalies between the Amundsen and Bellingshausen sectors (dashed oblique lines in Fig. 7a, b). On the slope and east of 120° W, advection is eastward (Fig. 8) and onshore heat transport is largest at this location. Signs of eastward propagation are apparent in the

Hovmöller diagrams (Fig. 7a, b), albeit more ambiguous than signs of westward propagation. Eastward propagation is also supported by the large signals that emerge in the Bellingshausen sector ca. 9 years after temperature anomalies arise in the Amundsen sector (Fig. 6c). To elucidate the physical mechanism behind the eastward propagation, we show the lagged regression of temperature anomalies in the 200–400-, 400–600-, and 600–800-m layers in the wider Southern Ocean onto the shelf-averaged temperature. We have chosen to show anomalies in these three layers as the mechanism involves vertical advection and mixing between the layers as well (Fig. 9). We infer that eastward propagation of temperature anomalies from the Amundsen to the Bellingshausen sector is due to a combination of two mechanisms: (i) eastward advection along the slope mainly below 400 m depth (Fig. 9b, c, but also compare Fig. 9a with Fig. 6a for context), upwelling, and southward on-shelf transfer near 75° W (Figs. 8a, b and 9d–f); and (ii) above 400 m depth, eastward advection to the north of the slope via southern branches of the Antarctic Circumpolar Current (Fig. 9e ,f) to the point at which the shelf break turns northward, east of 75° W. These two mechanisms operate in succession and together have a time scale of ~ 8 years. We find no signs of eastward advection along the tip of the Antarctic Peninsula.

Both westward propagation speeds seem to imply a faster connection between Amundsen and Ross sectors than the lag of 9 years inferred from Fig. 6, although it should be stressed that this lag is based on time difference between Amundsen anomalies and redistribution of those along the whole Antarctic shelves and may as well be determined by the time scale of anomalies in the Amundsen sea, i.e., how fast they switch sign. That time scale is determined by the forcing, to be thought to originate from the tropical Pacific. To establish which propagation mode (slow along-shelf vs. fast along-slope) is most important in distributing temperature anomalies westward onto the Antarctic shelf, we consider, for various depth ranges, lagged regressions of meridionally averaged temperature anomalies on the shelf to the circumpolar shelf-averaged temperature (Fig. 10). In the 200–400-m layer, a signal of westward propagation from the Amundsen to the Ross sector stands out (Fig. 10a, b), both on the shelf and on the slope. A peak in the Bellingshausen sector is also visible ~ 8 years after the signal emerges in the Amundsen sector, consistent with the eastward propagation mechanism. Because the eastward pathways partly run off the slope, a continuous eastward propagation is not visible in Fig. 10a and b. Neither is there any suggestion of westward propagation from the Bellingshausen to the Amundsen sector of anomalies, only for westward propagation from the Amundsen sector to farther west. In the 600–800-m layer, not any propagation signal is visible (Fig. 10c, d). There are positive anomalies in this depth range before the

shelf-averaged temperature peaks and negative anomalies afterwards; however, such anomalies appear almost simultaneously, without a clear propagation signal. We infer that the faster westward propagation mode along the slope does not correlate with the shelf-averaged temperature time series, and thereby, the regression maps highlight a dominance of the slow advective mode along the shelf in propagating anomalies. Fig. 10a also reconciles the slight difference between the 7-year advection time scale associated with the slow propagation model and the 9-year lag inferred from Fig. 4. Also, Fig. 10a supports 9-year lag, but at the same time, it also supports a 7-year advection time scale. It takes ~ 2 years before the anomaly that first appears in the eastern Amundsen sector has been carried to its western part before advection to sectors farther west start being effective. From Fig. 8a and b, we infer that the eastward undercurrent advects slope water to the eastern part of the Amundsen sector, after which it recirculates on the shelf to feed the westward flowing Antarctic Slope Current 2 years later.

4.3 The connection between the shelf and the slope

The connection between shelf and slope anomalies is focussed on depths less than 600 m (Fig. 8a, b) but, once on the shelf, the shallower anomalies also feed deeper troughs. Temperature anomalies on the slope feed the shelf between 120° W and 100° W via an eastward undercurrent along the slope in the Amundsen Sea, which turns southward onto the shelf between 110° W and 100° W (Fig. 8a, b) (Jenkins et al. 2016). Thereafter, these anomalies propagate farther westward via the slow mode (Antarctic Coastal Current). Farther west, anomalies on the shelf on their turn can feed the slope via north-westward-flowing currents (Fig. 8a, b). Hence, when anomalies primarily propagate along the shelf and, in addition, are transferred from the shelf to the slope, the slower propagation mode dominates on both the shelf and slope (Fig. 7a–d). If, in contrast, anomalies primarily propagate along the slope and, in addition, are transferred from the slope to the shelf, the faster propagation mode dominates. This is always the case in the 600–800-m layer (Fig. 7e, f), but occasionally at shallower depths too, especially when on-shelf anomalies flow back toward the slope at 125° W (Fig. 7a, b). West of 125° W, the Antarctic Slope Current carries on-shelf anomalies farther westward (Fig. 8a, b), but these anomalies remain confined to the northern edge of the shelf as far as 170° W. Upon reaching that longitude, anomalies are redirected along a trough connecting to the southern part of the shelf's Ross sector (Fig. 8a, b).

Figs. 6 and 10a and b indicate that the Amundsen sector stands as the gateway through which upwelling of deep anomalies onto the slope and shelf primarily takes place. To investigate this assertion further, we calculate the lagged regression between local shelf anomalies and slope anomalies
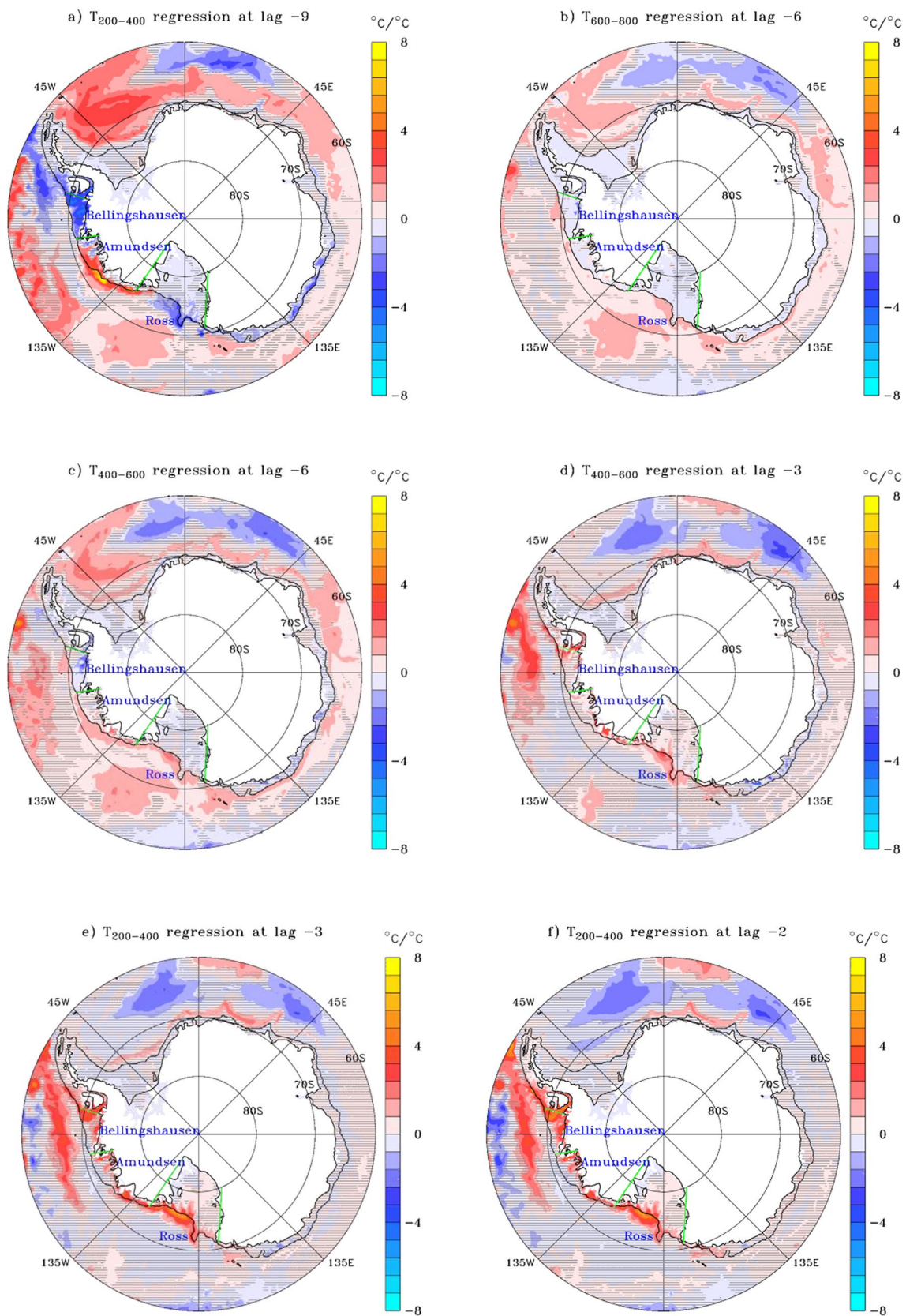
Fig. 9 Regression of vertically integrated temperature over **a**, **e**, **f** 200–400 m depth; **c**, **d** 400–600 m depth; and **b** 600–800 m depth onto the shelf-averaged and vertically integrated temperature anomaly at **a** lag − 9 years; **b**, **c** at lag − 6 years; **d**, **e** at lag − 3 years; and **f** at lag − 2 years (units in °C °C^{-1}). Non-significant values according to a two-sided Student *T*-test are overlaid by grey horizontal lines
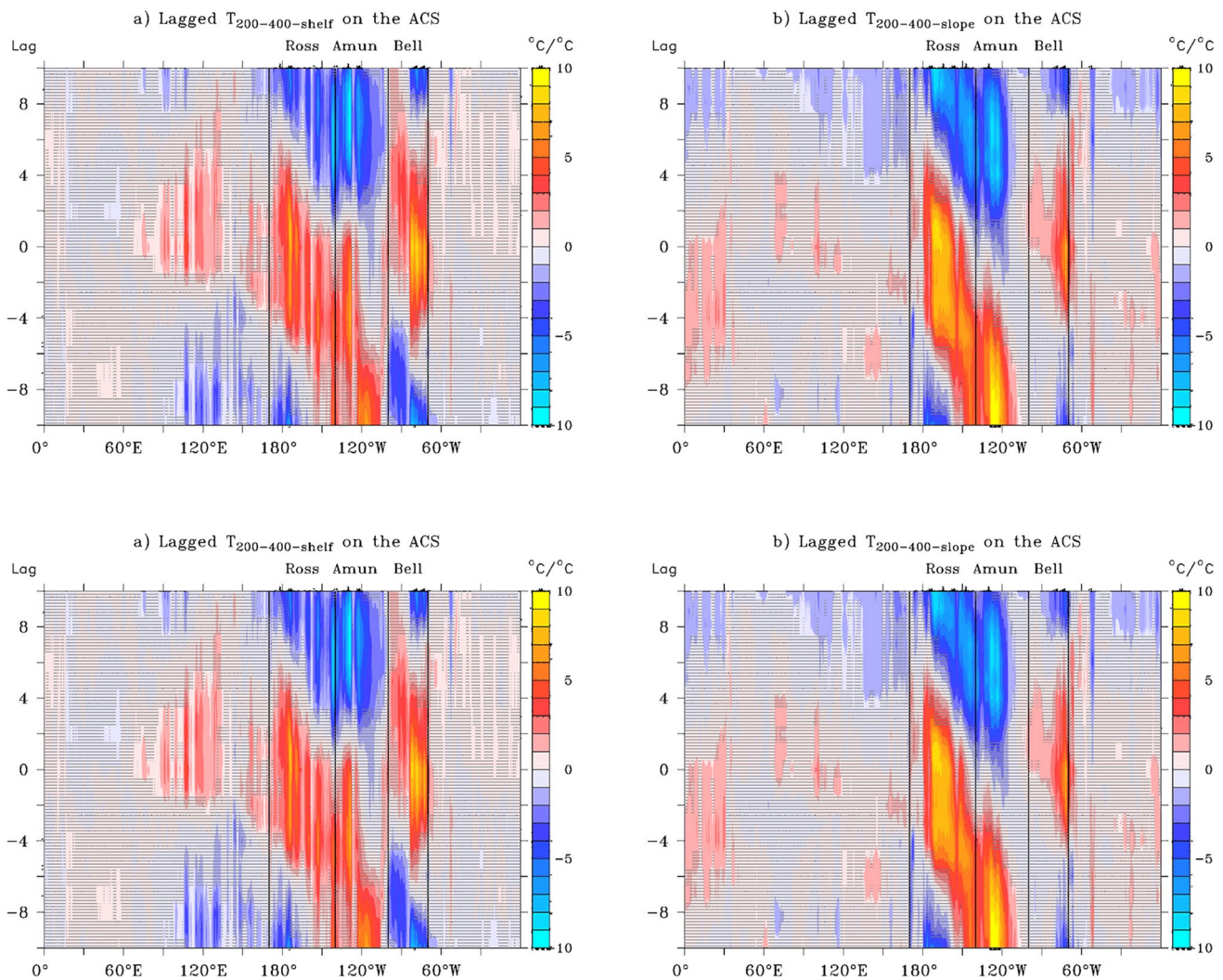
Fig. 10 Lagged regression of **a** shelf temperature averaged over a 2° latitude band south of the shelf edge and **b** slope temperature averaged over a 2° latitude band north of the shelf edge, averaged over **a**, **b** 200–400 m depth; **c**, **d** 200–400 m depth; and **e**, **f** 600–800 m depth, on depth-averaged temperature over the whole Antarctic shelf (units are 0.1 °C °C⁻¹). Non-significant values according to a two-sided Student **T**-test are overlaid by grey horizontal lines

in the Amundsen sector averaged between 140° W and 100° W (Fig. 11a). The connection between local shelf anomalies to the west of the Amundsen sector and anomalies over the slope in the Amundsen sector becomes important with increasing lag (Fig. 11a), with much larger amplitudes in the Ross sector than when anomalies are regressed to slope anomalies in the Ross sector itself (Fig. 11c). This is in agreement with the dominance of the slow advection mode indicated in Figs. 8 and 10a and b. It implies that heat reaches the continental shelf at 140° W–100° W and is then mostly redistributed by the slow (shelf) mode. Further, the signal in the Bellingshausen sector arises after ~ 8 years, consistent with the eastward propagation pathway north of the shelf that connects the eastern Amundsen and Bellingshausen sectors. In contrast, anomalies in the Antarctic shelf outside the Bellingshausen sector do not originate

from off-shelf anomalies in the Bellingshausen Sea (Fig. 11b): upwelling of anomalies in the Bellingshausen sector is only locally important, and these anomalies do not propagate further. Fig. 11c corroborates the assertion that the Amundsen Sea is a hotspot for upwelling onto the slope and shelf, by showing the lagged regression between local shelf and local slope anomalies at each longitude. The regression peaks when the shelf lags the slope by 1 year.

5 Discussion and conclusions

This study endorses the view of the Amundsen sector of the Antarctic shelf as the most sensitive to decadal wind-forced ocean variability. Changes in heat content occur with
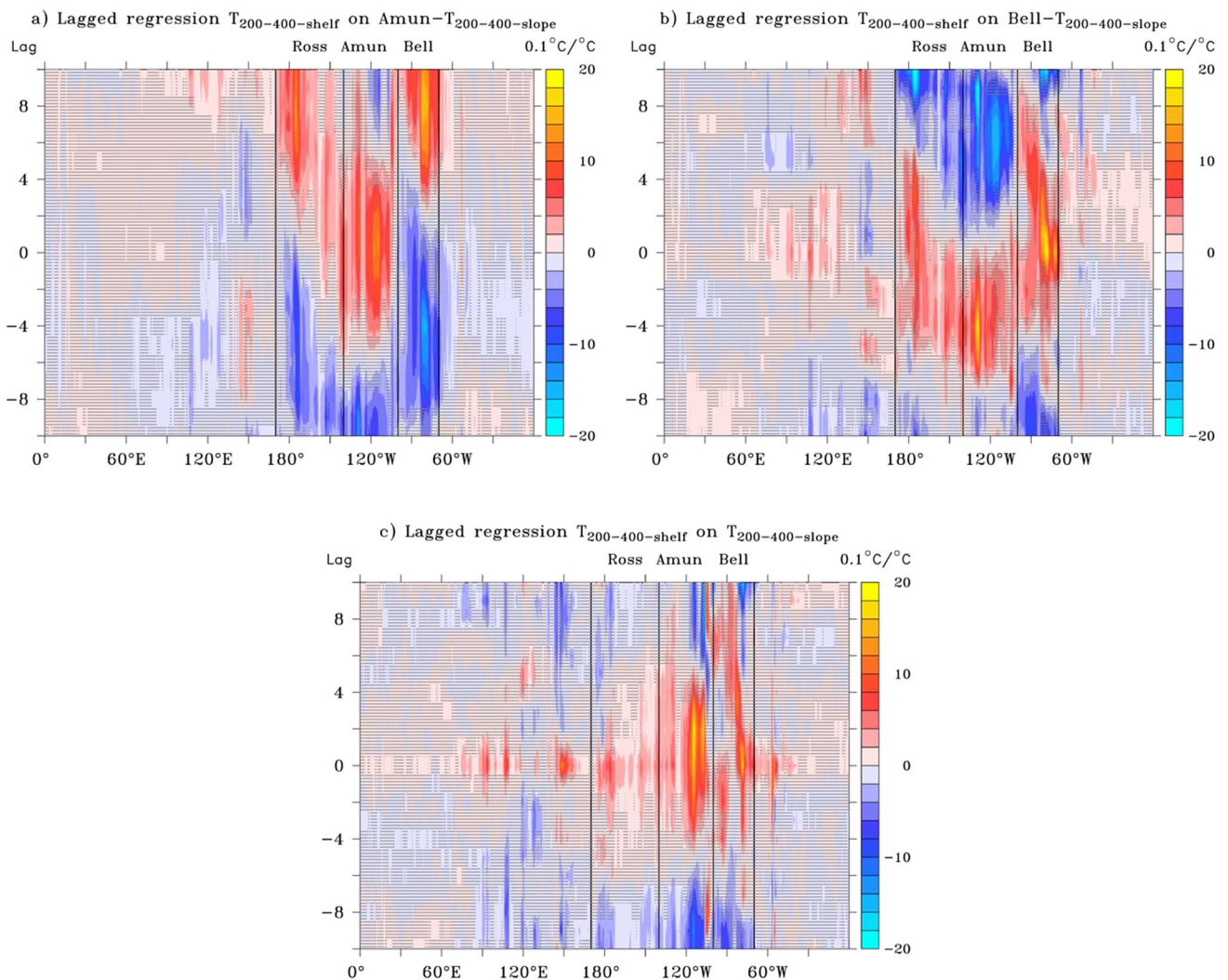
Fig. 11 Lagged regression of shelf temperature averaged over a 2° latitude band south of the shelf break and 200–400 m depth, on the 200–400-m depth-averaged temperature on the slope averaged over a 2° latitude band and **a** averaged over the Amundsen sector, **b** average over the Bellingshausen sector, **c** no domain average (units in 0.1 °C °C^{-1}). Non-significant values according to a two-sided Student T-test are overlaid by grey horizontal lines

a dominant decadal time scale driven by tropical climate variability, via the regulation of CDW intrusions onto the shelf via shifts in position and intensity of the Amundsen Sea Low (see Supplementary Information and Supplementary Fig. 3). The key new element put forward by this study is the Amundsen Sea's role as a gateway regulating the on-shelf access of CDW and its redistribution to other sectors of the Antarctic shelf. The import of Amundsen-sourced temperature anomalies can be as influential as the generation of anomalies by changes in local upwelling. We found that CDW access on the shelf is mainly accomplished by an eastward undercurrent along the slope in the Amundsen sector that turns southward on the shelf. Part of the advected anomalies recirculates in the Amundsen sector until they are advected farther westward along a convoluted pathway by

the Antarctic Coastal Current (the slow propagation mode) or feed into the Antarctic Slope Current that starts to develop in the western part of the Amundsen sector via a fast propagation mode, in which slope water intermittently floods the shelf via deep troughs west of the Amundsen sector. The timing of variations in heat content in the Ross sector and averaged over the whole Antarctic continental shelf complies with the slow propagation mode and eastward propagation of Amundsen sector anomalies to the Bellingshausen sector via a pathway that involves southward branches of the Antarctic Circumpolar Current and runs partly north of the continental shelf and slope.

This storyline complements other previously described mechanisms focusing on the role poleward-shifting circumpolar winds (Spence et al. 2014) and variations in the

Southern Annular Mode (Verfaillie et al. 2022). It should be noted that also sea ice and glacial meltwater have been noted to spread westward from the Amundsen Sea (Assmann et al., 2005; Nakayama et al. 2020); however, these studies concern the spread of near-surface features, while we concentrate on water mass characteristics in the 200–800-m depth layer. The interaction between tropical climate variability and circumpolar winds is sometimes characterised as the Pacific-South American (PSA) mode of variability (Lou et al. 2021), and the SLP anomaly associated with warming of the Amundsen sector coincides with the PSA's southern centre. The emergence of same-signed anomalies ~ 8 years later in the Bellingshausen sector can be explained by the eastward advection of eastern Amundsen-sourced anomalies along and to the north of the continental slope, whence the anomalies are transferred onto the shelf near 75° W. Here, they are reinforced by shallower anomalies that originate farther north in the Bellingshausen Sea, and that can be associated with the eastward propagation of the PSA (Lou et al. 2021) and a poleward shift of westerly winds (Spence et al. 2014). It is interesting to note that similar connectivity between the Amundsen and Ross sectors found in our study was also found for spreading of glacial meltwater (Nakayama et al. 2014) supporting our main findings, although we did not consider anomaly propagation in the 0–200-m depth layer, where the glacial meltwater mainly resides after upwelling below the floating ice shelf.

It should be noted that we have investigated only a 35-year model simulation containing about one-and-a-half cycle of the decadal variation present in the Amundsen Sea. We do not know whether the process documented here is also relevant for longer periods or whether it is relevant only for 1982–2017, as both climate change and/or changes in the phasing of the driving tropical variability may affect the variability on the Antarctic continental shelf. Further shortcomings of the model-data analysed are the absence of a spin-up before the model is initialised and forced with the JRA-55 data and the use of prescribed meltwater fluxes based on Rignot et al. (2013), instead of calculating those fluxes interactively. Unfortunately, either the model or the available basal melt parameterisations are not (yet) good enough to allow such an interactive calculation without creating strong biases in water mass characteristics on the Antarctic shelves Mathiot et al. 2017). Nevertheless, we believe that using the Rignot et al. (2013) fluxes is a reasonable alternative.

It could also be the case that details of the mechanism by which CDW variability is expressed on the Antarctic shelf change when higher-resolution processes are captured by a model (Stewart and Thompson 2015; Kimura et al. 2017; Stewart et al. 2018). Note, however, that, although our model's resolution is too coarse to resolve the eddy field on the shelf, most heat transport is channelled by troughs that support on-shelf geostrophic flow that is well captured by the model analysed. Also, using an eddying model, a recent analysis endorses the connectivity of the Antarctic shelf (Dawson et al. 2023), essential for the process considered here. While advection time scales are shorter in that model, with peak values between 1 and 5 years to travel 90° in longitude, by seeding many particles in the 0–200-m layer as well, their results are biased to larger current velocities compared to our study. Nevertheless, their result implies a faster and possibly stronger redistribution of Amundsen sector anomalies that could reach further west before anomalies within the Amundsen sector change sign when accounted for the stronger velocities that occur in a higher-resolution model. It would be interesting to repeat the present analysis with their model to check whether the lag between the Amundsen sector and circumpolar-averaged Antarctic shelf temperature anomalies indeed becomes shorter.

Declarations

Competing interests The authors declare no competing interests.

References

Assmann KM, Hellmer HH, Jacobs SS (2005) Amundsen Sea ice production and transport. J Geophys Res 110:C12013. https://doi.org/10.1029/2004JC002797

Assmann KM et al (2013) Variability of circumpolar deep water transport onto the Amundsen Sea continental shelf through a shelf break trough. J Geophys Res Oceans 118:6603–6620

Auger M et al (2021) Southern Ocean in-situ temperature trends over 25 years emerge from interannual variability. Nat Commun 12:514

Bowen MM, Fernandez D, Forcen-Vazquez A et al (2021) The role of tides in bottom water export from the western Ross Sea. Sci Rep 11:2246

Bronselaer B et al (2020) Importance of wind and meltwater for observed chemical and physical changes in the Southern Ocean. Nat Geosci. 13:35–42

Bull CYS et al (2021) Remote control of filchner-ronne ice shelf melt rates by the antarctic slope current. J Geophys Res Oceans 126(2):e2020JC016550

Cai W et al (2023) Antarctic shelf ocean warming and Sea ice melt affected by projected El Niño changes. Nat Clim Chang 13:235–239

Dawson HRS, Morrison AK, England MH, Tamsitt V (2023) Pathways and timescales of connectivity around the Antarctic continental shelf. J Geophys Res Oceans 128:e2022JC018962

Dotto TS et al (2019) Wind-driven processes controlling oceanic heat delivery to the Amundsen Sea. Antarctica J Phys Oceanogr 49:2829–2849

Fogt RL, Marshall GJ (2020) The Southern Annular mode: variability, trends, and climate impacts across the Southern Hemisphere. WIREs Clim Change 11:e652

Good SA, Martin MJ, Rayner NA (2013) EN4: quality controlled ocean temperature and salinity profiles and monthly objective analyses with uncertainty estimates. J Geophys Res-Oceans 118:6704–6716. https://doi.org/10.1002/2013JC009067

Heuzé C (2021) Antarctic bottom water and North atlantic deep water in CMIP6 models. Ocean Sci 17:59–90. https://doi.org/10.5194/os-17-59-2021

Holland PR, Bracegirdle TJ, Dutrieux P, Jenkins A, Steig EJ (2019) West Antarctic ice loss influenced by internal climate variability and anthropogenic forcing. Nat Geosci 12:718–724

Jenkins A, Jacobs S (2008) Circulation and melting beneath George VI Ice Shelf, Antarctica. J Geophys Res 113:C04013. https://doi.org/10.1029/2007JC004449

Jenkins A et al (2016) Decadal ocean forcing and Antarctic ice sheet response: lessons from the Amundsen Sea. Oceanogr. 29:106–117

Jenkins A et al (2018) West Antarctic ice sheet retreat in the Amundsen Sea driven by decadal oceanic variability. Nat Geosci 11:733–738

Jeong H et al (2020) Impacts of ice-shelf melting on water-mass transformation in the Southern Ocean from E3SM simulations. J Clim 33:5787–5807

Kimura S et al (2017) Oceanographic controls on the variability of ice-shelf basal melting and circulation of glacial meltwater in the Amundsen Sea Embayment, Antarctica. J Geophys Res Oceans 122:10131–10155

Lou J, O'Kane TJ, Holbrook NJ (2021) Linking the atmospheric Pacific-South American mode with oceanic variability and predictability. Commun Earth Environ. 2:223

Madec G (2016) NEMO Ocean Engine. Scientific notes of climate modelling center Institute Pierre-Simon Laplace 27:1288–1619

Mathiot P, Jenkins A, Harris C, Madec G (2017) Explicit representation and parametrised impacts of under ice shelf seas in the z∗ coordinate ocean model NEMO 3.6. Geosci Model Dev. 10:2849–2874

Meredith M et al (2019) in *IPCC special report on the ocean and cryosphere in a changing climate* (eds Pörtner, H.-O. et al.)

Moorman R, Morrison AK, Hogg AMC (2020) Thermal responses to Antarctic ice shelf melt in an eddy-rich global ocean–sea ice model. J Clim. 33:6599–6620

Nakayama Y et al (2014) Modeling the spreading of glacial meltwater from the Amundsen and Bellingshausen Seas. Geophys Res Lett 41:7942–7949. https://doi.org/10.1002/2014GL061600

Nakayama Y, Timmermann R, Hellmer H (2020) Impact of West Antarctic ice shelf melting on Southern Ocean hydrography. The Cryosphere 14:2205–2216. https://doi.org/10.5194/tc-14-2205-2020

Naughten KA et al (2022) Simulated twentieth-century ocean warming in the Amundsen Sea, West Antarctica. Geophys Res Lett 49:e2021GL094566

Neme J, England MH, Hogg AM (2021) Seasonal and interannual variability of the Weddell gyre from a high-resolution global ocean-sea ice simulation during 1958–2018. J Geophys Res Oceans 126(11):017662

Orsi AH, Whitworth III T (2005) *Hydrographic atlas of the World Ocean Circulation Experiment (WOCE): volume 1. Southern Ocean*. M. Sparrow, P. Chapman, and J. Gould, eds, International WOCE Project Office, Southampton, UK

Paolo FS, Fricker HA, Padman L (2015) Volume loss from Antarctic ice shelves is accelerating. Science 348:327–331

Pritchard HD et al (2012) Antarctic ice-sheet loss driven by basal melting of ice shelves. Nature 484(7395):502. https://doi.org/10.1038/nature10968

Rignot E, Jacobs S, Mouginot J, Scheuchl B (2013) Ice-shelf melting around Antarctica. Science 341:266–270

Sallée J-B (2018) Southern Ocean warming. Oceanogr 31:52–62

Rousset C et al (2015) The Louvain-La-Neuve sea ice model LIM3.6: Global and regional capabilities. Geosci Model Dev 8:2991–3005

Schmidtko S, Heywood KJ, Thompson AF, Aoki S (2014) Multidecadal warming of Antarctic waters. Science 346(6214):1227–1231

Spence P et al (2014) Rapid subsurface warming and circulation changes of Antarctic coastal waters by poleward shifting winds. Geophys Res Lett 41:4601–4610

Stewart AL, Klocker A, Menemenlis D (2018) Circum-Antarctic shoreward heat transport derived from an eddy- and tide-resolving simulation. Geophys Res Lett 45:834–845

Stewart AL, Thompson AF (2015) Eddy-mediated transport of warm Circumpolar Deep Water across the Antarctic shelf break. Geophys Res Lett 42:432–440. https://doi.org/10.1002/2014gl062281

St-Laurent P, Klinck JM, Dinniman MS (2015) Impact of local winter cooling on the melt of Pine Island Glacier Antarctica. J Geophys Res Oceans 120:6718–6732

Storkey D et al (2018) UK Global Ocean GO6 and GO7: a traceable hierarchy of model resolutions. Geosci Model Dev 11:3187–3213

Thompson AF, Stewart AL, Spence P, Heywood KJ (2018) The Antarctic Slope Current in a changing climate. Rev Geophys 56:741–770

Timmermann R, Hellmer HH (2013) Southern Ocean warming and increased ice shelf basal melting in the twenty-first and twenty-second centuries based on coupled ice-ocean finite-element modelling. Ocean Dyn. 63:1011–1026

Tsujino H et al (2018) JRA-55 based surface dataset for driving ocean-Sea-ice models (JRA55-do). Ocean Modelling 130:79–139

Verfaillie D et al (2022) The circum-Antarctic ice-shelves respond to a more positive Southern Annular Mode with regionally varied melting. Commun Earth Environ 3:139

Walker DP et al (2013) Oceanographic observations at the shelf break of the Amundsen Sea Antarctica. J Geophys Res Oceans 118:2906–2918

Webber BGM et al (2017) Mechanisms driving variability in the ocean forcing of Pine Island Glacier. Nat Commun. 8:14507